Materials Science & Engineering C 126 (2021) 112175

Contents lists available at ScienceDirect

Materials Science & Engineering C

journal homepage: www.elsevier.com/locate/msec

Polysaccharides on gelatin-based hydrogels differently affect chondrogenic differentiation of human mesenchymal stromal cells

Luciana Sartore [a], Cristina Manferdini [b], Yasmin Saleh [b], Kamol Dey [a,c], Elena Gabusi [b], Giorgio Ramorino [a], Nicoletta Zini [d,e], Camillo Almici [f], Federica Re [g], Domenico Russo [g], Erminia Mariani [b,h], Gina Lisignoli [b,*]

[a] Dipartimento di Ingegneria Meccanica e Industriale, Università degli Studi di Brescia, Via Branze 38, 25123 Brescia, Italy
[b] IRCCS Istituto Ortopedico Rizzoli, SC Laboratorio di Immunoreumatologia e Rigenerazione Tissutale, via di Barbiano 1/10, 40136 Bologna, Italy
[c] Department of Applied Chemistry and Chemical Engineering, Faculty of Science, University of Chittagong, Chittagong-4331, Bangladesh
[d] CNR Institute of Molecular Genetics "Luigi Luca Cavalli-Sforza", Unit of Bologna, via di Barbiano 1/10, 40136 Bologna, Italy
[e] IRCCS Istituto Ortopedico Rizzoli, via di Barbiano 1/10, 40136 Bologna, Italy
[f] Laboratory for Stem Cells Manipulation and Cryopreservation, Department of Transfusion Medicine, ASST Spedali Civili, P.le Spedali Civili 1, 25123 Brescia, Italy
[g] Unit of Blood Disease and Bone marrow Transplantation, DPT of Clinical and Experimental Science, Brescia University and ASST Spedali Civili of Brescia, P.le Spedali Civili 1, 25123 Brescia, Italy
[h] DIMEC, Alma Mater Studiorum, Università di Bologna, via Massarenti 9, 40138 Bologna, Italy

ARTICLE INFO

Keywords:
Chitosan/dextran-based scaffold
Stress relaxing hydrogel
Human mesenchymal stromal cells
Tissue engineering
Cartilage regeneration

ABSTRACT

Selection of feasible hybrid-hydrogels for best chondrogenic differentiation of human mesenchymal stromal cells (hMSCs) represents an important challenge in cartilage regeneration. In this study, three-dimensional hybrid hydrogels obtained by chemical crosslinking of poly (ethylene glycol) diglycidyl ether (PEGDGE), gelatin (G) without or with chitosan (Ch) or dextran (Dx) polysaccharides were developed. The hydrogels, namely G-PEG, G-PEG-Ch and G-PEG-Dx, were prepared with an innovative, versatile and cell-friendly technique that involves two preparation steps specifically chosen to increase the degree of crosslinking and the physical-mechanical stability of the product: a first homogeneous phase reaction followed by directional freezing, freeze-drying and post-curing. Chondrogenic differentiation of human bone marrow mesenchymal stromal cells (hBM-MSC) was tested on these hydrogels to ascertain whether the presence of different polysaccharides could favor the formation of the native cartilage structure. We demonstrated that the hydrogels exhibited an open pore porous morphology with high interconnectivity and the incorporation of Ch and Dx into the G-PEG common backbone determined a slightly reduced stiffness compared to that of G-PEG hydrogels. We demonstrated that G-PEG-Dx showed a significant increase of its anisotropic characteristic and G-PEG-Ch exhibited higher and faster stress relaxation behavior than the other hydrogels. These characteristics were associated to absence of chondrogenic differentiation on G-PEG-Dx scaffold and good chondrogenic differentiation on G-PEG and G-PEG-Ch. Furthermore, G-PEG-Ch induced the minor collagen proteins and the formation of collagen fibrils with a diameter like native cartilage.

This study demonstrated that both anisotropic and stress relaxation characteristics of the hybrid hydrogels were important features directly influencing the chondrogenic differentiation potentiality of hBM-MSC.

1. Introduction

The treatment of cartilage degeneration is a complex clinical problem, and the need for effective methods to replace or integrate parts of the cartilage tissue remains an unsolved issue. The injury or loss of cartilage tissue can be a consequence of trauma or physiological wear, especially in athletes or people who utilize knee cartilage more intensely and for longer period. Articular cartilage lesions generally do not heal, due to the lack of nerves, blood vessels and a lymphatic system [1,2]. The limited reparative capabilities of articular cartilage (hyaline

* Corresponding author at: IRCCS Istituto Ortopedico Rizzoli, SC Laboratorio di Immunoreumatologia e Rigenerazione Tissutale, via di Barbiano 1/10, 40136 Bologna, Italy.
E-mail address: gina.lisignoli@ior.it (G. Lisignoli).

https://doi.org/10.1016/j.msec.2021.112175
Received 21 January 2021; Received in revised form 28 April 2021; Accepted 4 May 2021
Available online 8 May 2021

cartilage) usually results in the generation of fibrocartilage tissue that lacks the structure and biomechanical properties of healthy cartilage and degrade over the course of time. Currently, the most widely utilized techniques for cartilage defects, and degeneration are not articular cartilage substitution procedures, but rather lavage, arthroscopic debridement, and repair stimulation. Arthroscopic washing involves the use of irrigating solutions into the joint that eliminate degenerative cartilage debris and can provide temporary pain relief but have little or no chance of definitive repair and healing. Repair stimulation is conducted by means of drilling, abrasion arthroplasty or microfracture. Penetration into the subchondral bone induces bleeding and formation of fibrin clot which promotes initial repair of the cartilage. However, the newly generated tissue has a fibrous and not durable nature; it degenerates and presents loss of resilience, stiffness, and wear characteristics over time. Although several methods are currently known, the treatment of joint cartilage degeneration remains a difficult clinical problem showing the regenerated cartilage fibro-hypertrophic characteristics [3].

Tissue engineering could represent a possible solution for the repair and regeneration of these tissues [4]. The development of new engineered scaffolds that, implanted in the body can temporarily compensate for the impaired function and stimulate the regrowth of damaged tissue, represents a challenge for researchers. To address this issue, scaffold-based tissue engineering attempts to recapitulate native cartilage-like microenvironment to stimulate chondrogenesis. Remarkably, for successful cartilage tissue repair, a sagacious selection of biomaterial is also crucial. Native articular cartilage niche comprises chondrocytes and a specialized extra cellular matrix (ECM) mainly composed of collagen that form a network with linear heteropolysaccharide glycosaminoglycans (GAGs) [5–7]. Collagen type II is the major component of ECM (approximately 90%) in mature articular cartilage, with smaller amounts of collagen type XI (3%) and IX (1%) [8,9]. This specialized ECM provides unique mechanical properties of cartilage tissue including, stress management, wear-resistance and load-bearing capability without being damaged [10]. While collagen plays the pivotal role in structural and load-bearing performance, thanks to its strain-stiffening effect, surrounding polysaccharide elastically reinforces collagen and synergistically participates in internal stress management [11]. Apart from mechanical contribution, polysaccharide allows to absorb substantial water and various fluids, because of its highly hydrophilic nature, resulting in a smooth and lubricated surface that facilitates load transmission with a low frictional coefficient [10]. Altogether, a hybrid - protein plus polysaccharide - scaffolding material may appear as a potential platform for chondrogenic differentiation of stem cell.

Numerous polysaccharides including, hyaluronic acid, chondroitin sulphate, chitosan, alginate and agarose, demonstrate their potentiality as biomaterials for cartilage tissue engineering due to the engagement of saccharide unit in cell signalling, among other advantageous factors [12,13]. However, chitosan (Ch), a derivative of the alkaline deacetylation of chitin, stands top in the polysaccharide list, because of being biocompatible, biodegradable, bacteriostatic, hemostatic, non-toxic, and bioactive and having structural similarity to glycosaminoglycan (GAG), and processability to porous scaffolds, films and beads [14,15]. On the other hand, dextran (Dx) an easily available polysaccharide and its derivatives, appears to be shown in biomedical application, particularly, towards angiogenesis and wound healing process [16–19]. Though, Dx-based hydrogels have been successfully used for cartilage tissue regeneration, but they are mostly 3D unstructured products (injectable hydrogels and microcarrier) [20–23].

In a previous study, we compared the physicomechanical properties and the degree of chondrogenesis of a novel gelatin (G)-polyethylene glycol (PEG) hydrogel alone and with different quantities of Ch with the aim of identifying the most favourable conditions for cartilage tissue regeneration [24]. We demonstrated that high concentration of Ch in combination with TGFβ3 chondrogenic factors create an environment that induced human bone marrow mesenchymal stromal cells (hBM-MSCs) chondrogenic differentiation by recapitulating specific phases that have contribute to increase chondrogenic markers associated with a decrease of hypertrophic and fibrotic markers [24].

Following this excellent result and considering the role of anisotropy in cartilage tissue regeneration [25–27] that impact on cell phenotype and function [28,29], we investigated the extent of chondrogenic differentiation of hBM-MSCs in response to the degree of elastic anisotropy of different hydrogels. In the present study, we aimed to clarify the role of the polysaccharide as well as physicomechanical properties on chondrogenesis, on three hydrogels that shared the same backbone of G-PEG, with a constant ratio of G/PEG (equal to 4.2), without or with the same amount of two different polysaccharides, namely, Ch (G-PEG-Ch) and Dx (G-PEG-Dx).

2. Materials and methods

2.1. Polysaccharides hybrid hydrogels preparation

The hybrid hydrogels were synthesized using a developed methodology in our laboratory [30]. Briefly, 6 g of type A gelatin (G) (pharmaceutical grade, 280 bloom, viscosity 4.30 mPs, produced from pig skin, Italgelatine, Cuneo, Italy) was dissolved in 65 ml distilled water at 40 °C and then stirred, followed by dropwise addition of 1.4 g poly (ethylene glycol) diglycidyl ether (PEGDGE, molecular weight 526 Da, Sigma-Aldrich Co, Milan, Italy) and 70 mg ethylene diamine (EDA, Fluka, Milano, Italy). To obtain G-PEG hydrogel, the reaction mixture was gently stirred at 40 °C for 20 min and poured into the glass plate for gel formation. The gel was then cut into a rectangular bar and placed into pyrex crystallizing dish. The direction-dependent freezing was done by resting the crystallizing dish on the surface of 8-cm-deep pool of liquid nitrogen, enabling freeze-casting at −196 °C. Freezing was visually assessed. During the evaporation of liquid nitrogen, the gel was unidirectionally frozen from the bottom to the top. The gel was incubated for 30 min at the freezing temperature for ensuring complete freezing. Subsequently, the frozen gel was transferred to the freeze-dryer (lyophilizer), operating under vacuum at -60 °C, for sublimation of ice crystals, resulting in an anisotropic porous dry material. Finally, the porous material was post-cured at 45 °C for 2 h in the oven under vacuum to complete crosslinking or grafting reactions. The freeze-dried gel was washed several times with distilled water at 37 °C to eventually remove the unreacted reagents and soluble components and finally freeze-dried in lyophilizer. In order to prepare G-PEG-Ch and G-PEG-Dx hydrogels, the required amounts of chitosan (Ch = 16 wt%, molecular weight between 50,000–190,000 Da and degree of deacetylation 75–85%, Fluka) (2 wt% solution in acetic acid) and dextran (16 wt%) was individually dissolved into the G-PEG reaction mixture. The final reaction mixture was gently stirred at 40 °C for 20 min to obtain homogeneous mixture, poured into the glass plate for gel formation and then followed the above stated steps. Fig. 1a shows the preparation scheme of hybrid anisotropic hydrogels G-PEG, G-PEG-Ch and G-PEG-Dx. The composition and physical properties of the hydrogels are reported in Table 1. 100 cylindrical samples (D = 8 mm h = 5 mm) of each hydrogel compositions were cut by mechanical saw in dry state and packed into polypropylene bag and sealed under vacuum. Packed hydrogel scaffold samples were sterilized by gamma irradiation with Cobalt 60 gamma rays using 27–33 kGy following UNI EN ISO 11137 (Sterilization of Health Care Products).

2.2. Chemical, morphological and mechanical characterization of hybrid hydrogels

Fourier transform infrared (FTIR) spectra were obtained on dry hydrogels using a Thermo Scientific, Nicolet iS50 FTIR spectrophotometer (Thermo Fisher Scientific, Madison, Wisconsin, USA) equipped with a PIKE MIRacle attenuated total reflectance attachment and

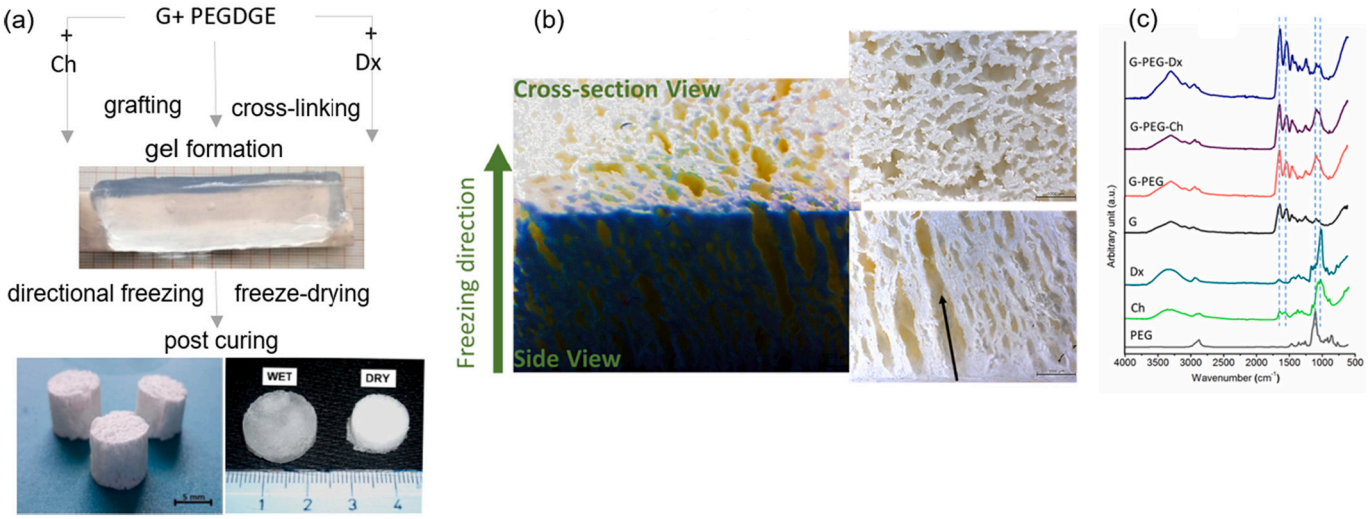

Fig. 1. (a) Preparation scheme of hybrid anisotropic hydrogels G-PEG, G-PEG-Ch and G-PEG-Dx. (b) Optical microscopy of the hybrid hydrogels showing porous structure in perpendicular (cross-section view) and parallel (side view, the black arrow indicates the direction of macroporous channels) directions in the dried condition (scale bars: 1 mm). (c) FTIR spectra of pure components and final hydrogels.

Table 1
The composition and physical properties of the hybrid hydrogels.

Hydrogel	Composition (wt%)				Physical properties			
	G	PEG	CH	Dx	Apparent density [g cm^{-3}]	Porosity [%]	Mean pore sizes[a] (μm)	Ranges of pore sizes[a] (μm)
G-PEG	81	19	–	–	0.16 ± 0.01	75 ± 2	247 ± 80	50÷320
G-PEG-Ch	68	16	16		0.10 ± 0.02	81 ± 7	310 ± 75	50÷400
G-PEG-Dx	68	16		16	0.11 ± 0.02	78 ± 4	235 ± 87	80÷470

[a] Mean pore sizes and ranges of pore dimensions were evaluated on dry hydrogels; the pore size was evaluated in terms of pore diameter, as evaluated on 100 pores by means of an image analysis software (Image J).

recorded over a range of 400 to 4000 cm^{-1} at a resolution of 4 cm^{-1}.

Density and porosity of the dry samples were measured using liquid substitution method of Kothapalli et al. [31] using pure ethanol as the displacing liquid because it penetrates easily into the pores of the sample, without altering the structure itself.

The texture, morphology and porous structure of hydrogels were observed in both parallel and perpendicular directions using a stereomicroscope (LEICA DMS 300) with reflected light. The pore size was evaluated in terms of pore diameter, as evaluated on 100 pores by means of an image analysis software (Image J).

Compression and cyclic compression tests were carried out by an Instron series 3366 testing machine (INSTRON, Norwood, Massachusetts, USA), equipped with a 50 N load cell. The specimens were tested at room temperature after immersion in distilled water for 24 h at 37 °C (swollen condition). Samples were cut into rectangular specimens and compressed either in parallel or perpendicular to the macroporous channels at a strain rate of 10%/min up to 50% strain, then immediately unloaded. Before commencing the compression test, a load of 0.01 N was applied to ensure complete contact between the sample surface and plate. Ten consecutive loading-unloading cycles were applied without resting time. The dimension of the samples was measured using an optical travelling microscope. At least six specimens were tested for each hydrogel composition. Engineering stress and engineering strain were calculated using the dimensions of undeformed specimens, and the initial elastic modulus (stiffness) was determined from the slope of the initial linear segment of stress-strain curves. The energy absorption of the hydrogels was derived from the cyclic compressive stress-strain relations. Hysteresis loop area, bounded by the loading unloading curves, indicates the dissipated energy or adsorbed energy due to the viscous nature of the hydrogels. The compression energy (kJ/m^3), total energy applied to the hydrogel during compression, is defined as the area enclosed by loading curve and horizontal axis, while as, relaxation energy (kJ/m^3) is the area bounded between unloading curve and horizontal axis. The dissipation energy (kJ/m^3) loss during hysteresis cycle was calculated from the area bounded within hysteresis loop. The percentage of dissipation energy was determined by dividing the dissipation energy by the compression energy. The modulus anisotropy is defined as the ratio of elastic modulus in parallel to the perpendicular direction.

The stress-relaxation properties of the hydrogels were assessed by compression relaxation test. The pre-conditioned samples were quickly compressed to 15% strain with a deformation rate of 60 mm/min, and the strain was held constant up to 20 min, while the variation of stress was recorded as a function of time.

2.3. Hydrolytic mass loss evaluation and swelling ratio

The dry weighed (W_i) samples were incubated in distilled water at 37 °C over a three-week period. At regular intervals of 1, 10 and 21 days, the samples were removed, weighed (W_w), rinsed with fresh water, air dried followed by vacuum dried at 45 °C for 4 h, and finally dried mass (W_f) was measured. The swelling ratio (%) and mass loss (%) was calculated using following equations:

$$\text{Swelling ratio } (\%) = \left(W_w - W_f\right)/W_f \times 100$$

$$\text{Mass loss } (\%) = \left(W_i - W_f\right)/W_i \times 100$$

2.4. Chondrogenesis of human BM-MSCs on scaffolds

Human BM-MSCs were obtained from three different subjects, after scheduled BM harvests according to international standards and after

donor informed consent in accordance with the Declaration of Helsinki, expanded in culture with human platelet lysate and characterized as previously reported [24]. 1×10^6/100 μl hBM-MSCs were slowly seeded on G-PEG, G-PEG-Ch and G-PEG-Dx scaffolds of defined dimensions (5 mm width x 5 mm length x 4 mm height) in a 24-well non-adherent plate (Corning, Toledo, OH, USA) for 4 h at 37 °C. Cell adhesion to the scaffolds was checked by an inverted microscope (Nikon Instruments Europe BW) and the scaffolds were maintained in culture at 37 °C with 5% CO_2 in 2 ml of DMEM medium (Life Technologies). After 24 h, two milliliters of DMEM medium was substituted with control medium (CM) (high-glucose DMEM supplemented with 50 mg/ml ITS + premix, 10^{-7} M dexamethasone, 50 μg/ml ascorbate–2 phosphate, 1 mM sodium pyruvate and 100 U/ml-100 μg/ml penicillin-streptomycin, Sigma Aldrich) or with CM containing chondrogenic factor (TGF-β3, 10 ng/ml, Miltenyi Biotech, Auburn, CA, USA). Cell culture medium was changed twice a week.

2.5. Cell metabolic activity

Each construct was analysed for cell metabolic activity at days 1, 14, 28 and 48 by Alamar blue test. Briefly, the samples were incubated with 10% Alamar blue and after 4 h, the absorbance was read at 560 nm and 600 nm using automated spectrophotometric plate reader TECAN Infinite® 200 PRO (Tecan Italia S.r.l., Cernusco Sul Naviglio, Italy). The results were expressed as percentages of Alamar blue reduction, as indicated by the manufacturer's data sheet (Bio-Rad Laboratories).

2.6. Molecular biology analysis

Total RNA was extracted from all cell-scaffold samples at days 1 and 28 as previously reported [24]. Real time PCR was performed with LightCycler®2.0 (Roche Molecular Biochemicals, Mannheim, Germany) for the quantification of the following markers: Aggrecan (*ACAN*), SRY-Box Transcription Factor 9 (*SOX9*), Collagen type 1 alpha1 chain (*COL1A1*), Collagen type 2 alpha 1 chain (*COL2A1*), Collagen type 9 alpha 1 chain (*COL9A1*), Collagen type 11 alpha 1 chain (*COL11A1*), Cartilage oligomeric matrix protein (*COMP*), Metalloproteinase-13 (*MMP-13*), Collagen type 10 alpha 1 chain (*COL10A1*) (Table 2). Ribosomal protein 9 (RPS9) was tested as reference gene. Each sample was processed in duplicate. Relative expression levels for each target gene were calculated according to the formula $2^{-\Delta Ct}$, and expressed as fold change day 1 = 1.

2.7. Light microscopy analysis

On day 28 G-PEG, G-PEG-Ch and G-PEG-Dx scaffolds were fixed in 4% paraformaldehyde in PBS for 2 h, washed in PBS, dehydrated in ethanol, and embedded in paraffin. Sections of 5 μm were then stained for Toluidine blue/Haematoxylin-Eosin (Bioptica, Milan, Italy) and slides analysed by a light microscope according to the manufacturer instructions. To evaluate mineralization, we performed von Kossa staining. Briefly, sections were deparaffined, rehydrated and stained with 5% aqueous silver nitrate (Sigma-Aldrich, USA) solution under ultraviolet light for 30 min, rinsed in de-ionized water, immersed in 5% sodium thiosulfate solution (Sigma-Aldrich, USA) for 5 min RT and counterstained with haematoxylin. A positive control of hBM-MSCs osteogenic differentiated on biomaterial was included.

2.8. Transmission electron microscopy analysis

For ultrastructural evaluation, the scaffolds at day 48 were fixed in 2.5% glutaraldehyde in 0.1 M cacodylate buffer pH 7.4, 3 h at TA, then overnight at 4C° and processed as previously reported [24]. Ultrathin sections were stained with tannic acid, uranyl acetate and lead citrate, and observed with a Zeiss EM 109 transmission electron microscope (Zeiss, Oberkochen, Germany). Images were captured using a Nikon digital camera Dmx170 1200F and ACT-1 software. The quantitative image analysis of collagen fibrils diameters was performed on 10 images (original magnification x30000) using image analysis program Adobe photoshop CC 2017 (Adobe system). In each image we counted the total number of fibrils and calculated the frequency percentage of fibrils diameter of 10-19 nm, 20-29 nm, 30-39 nm, 40-49 nm and 50-59 nm as reported by Tanaka [32].

2.9. Statistical analysis

Statistical analysis was performed using non-parametric tests since the data did not have normal or strongly asymmetric distribution. Statistical analysis for metabolic activity data was performed using 2 ANOVA with Tukey's multiple comparisons test. For genes expression statistical analysis was performed Kruscall-Wallis ANOVA test with Dunn's for multiple comparison. Numerical and graphical results are presented as mean ± standard deviation (SD) with graphical results produced using GraphPad Prism (version 7.04). Significance was accepted at a level of $p < 0.05$ or $p < 0.01$.

Table 2
Oligonucleotide primers used for real-time PCR.

Name	Gene symbol	Ref_Seq	Primer sequences	Primer efficiency (%)
Aggrecan	*ACAN*	NM_001135	FW:TCGAGGACAGCGAGGCC REV:TCGAGGGTGTAGCTGTAGAGA	96,5
Cartilage oligomeric matrix	*COMP*	NC_000019.9 NG_007070.1 NT_011295.11	Biorad unique assay ID: qHsaCID0021064	95
Collagen type 1 alpha 1 chain	*COL1A1*	NM_000088	FW:CCTGGATGCCATCAAAGTCT REV:CGCCATACTCGAACTGGAAT	95,4
Collagen type 2 alpha 1 chain	*COL2A1*	NM_001844	FW:GACAATCTGGCTCCCAAC REV:ACAGTCTTGCCCCACTTAC	98,1
Collagen type 9 alpha 1 chain	*COL9A1*	NM_078485 NM_001851	FW:CAGGAAGAGGTCCCAAC REV:GCTGGCTCACAGAAACC	95
Collagen type 10 alpha 1 chain	*COL10A1*	NM_000493	FW:TGCTGCCACAAATACCCTTT REV:GTGGACCAGGAGTACCTTGC	96,8
Collagen type 11 alpha 1 chain	*COL11A1*	NC_000001.10 NT_032977.9 NG_008033.1	Biorad unique assay ID: qHsaCID0009011	98
Metallopeptidase 13	*MMP-13*	NM_002427	FW:TCACGATGGCATTGCT REV:GCCGGTGTAGGTGTAGA	92,5
SRY- Box Transcription factor 9	*SOX9*	NM_000346	FW:GAGCAGACGCACATCTC REV:CCTGGGATTGCCCCGA	97,2
Ribosomal protein 9	*RPS9*	NM_001013	FW:AAGTCCATCCACCACGCTC REV:GGAATCCAGGCGGACAATGA	94,1

3. Results

3.1. Anisotropic hybrid hydrogels preparation

At first, we synthesized anisotropic polysaccharide-based hybrid hydrogels using a very simple uniaxial freezing technique developed in our laboratory [30]. The crosslinking and grafting reactions between available functional groups (-NH_2, -COOH, -OH) of polymers (gelatin, chitosan and dextran) and crosslinking agent i.e. epoxy PEG were carried out using a facile but robust synthetic procedure in aqueous environment without using any additives or solvents followed by freeze drying technique. The developed protocol produced structurally stable hydrogels and allowed effective gamma sterilization of the samples without compromising their physicomechanical properties [33]. For imparting anisotropy, directional freeze-drying approach was adopted. During the liquid nitrogen-driven directional freezing (at -196 °C) of the gels, water molecule crystallizes to form aligned ice crystals template along the freezing direction, and the polymer chains rest in the gaps between them. The freeze-drying process under vacuum sublimates the ice crystals resulting in the interconnected macroporous channels along the freezing direction, as shown in Fig. 1b. While the cross-section view revealed highly interconnected irregular spherical pore morphology suggesting that the hybrid hydrogels have anisotropic architectures. Fig. 1c showed the FTIR analysis done on the samples after washing out the eventually un-reacted and soluble components. It was observed that all characteristic peaks of individual components are present in the final hydrogels indicating the hybrid nature of the prepared hydrogels. Particularly, the absorption peaks of 1631 and 1552 cm^{-1} which are corresponded to amide I and amide II, respectively, of the gelatin protein, while peak around 1096 cm^{-1} which is assigned to C—O stretching (ether bond C-O-C) confirm the presence of PEG in the final hydrogels. Additionally, incorporation of Ch and Dx polysaccharides contributes the band around 1080–1032 cm^{-1} [34].

The composition and the physical properties of the hybrid hydrogels were tabulated in the Table 1. The apparent density and porosity of the hybrid hydrogels was measured using ethanol displacement method. All hybrid hydrogels showed a high porosity of around 80% and based on the evaluation of pore diameters on images taken with the optical microscope, the pore size ranges between 50 and 470 μm with an average diameter ranging from 235 to 310 μm. The pores are thus on the average in line with the size requirement to ensure cell penetration, migration, and growth, as well as an optimal tissue vascularization. Moreover, the high porosity and hydrophilic nature of the constituent polymers enabled high water retention ability to all hydrogels, as shown in Fig. 2a. However, G-PEG-Ch and G-PEG-Dx showed higher amount of water uptake compared to that of G-PEG hydrogels, and the cause might be due to the lower cross-linking density (as confirmed by mechanical test) and higher hydrophilic nature of polysaccharides such as, Ch and Dx. Consequently, this higher water uptake and lower crosslinking density resulted in higher hydrolytic mass losses for G-PEG-Ch and G-PEG-Dx, as compared to G-PEG hydrogels, as shown in Fig. 2b.

3.2. Anisotropic mechanics and viscoelastic nature of the hybrid hydrogels

Fig. 3a shows the compressive stress-strain curves when compressed in parallel direction for all hybrid hydrogels. It was evident that incorporation of Ch and Dx into the G-PEG networks slightly reduced compressive elastic modulus (stiffness) of the hydrogels. The stiffness of the G-PEG, G-PEG-Ch and G-PEG-Dx hybrid hydrogels in parallel direction was found to be 0.33, 0.25 and 0.28 MPa, respectively, as shown in Table 3. The similar reduced trend was also visible for compression in perpendicular direction. Fig. 3b, c, d shows the direction-dependent compressive stress-strain curves for all hybrid hydrogels. All hydrogels display distinct stress-strain curves when they are compressed in parallel and perpendicular to the macroporous directions, indicating the anisotropic mechanics of the hydrogels. The elastic anisotropy, defined as the ratio of elastic modulus in parallel and perpendicular direction, for G-PEG, G-PEG-Ch and G-PEG-Dx hybrid hydrogels was found to be 2.8, 3.1 and 10.0, respectively. Interestingly, polysaccharide incorporation increased anisotropic ratio, particularly for dextran. G-PEG-Dx showed more than three times anisotropic ratio compared to that of parent G-PEG hybrid hydrogel.

Percentage dissipation energy and stress relaxation are two main features that indicate viscoelastic response of the material. We further investigated the cyclic compression test to measure the percentage dissipation energy, which is defined as the ratio of area between loading and unloading curves to the area covered by the loading curve, of the hybrid hydrogels. Table 3 shows the percentage dissipation energy of the hybrid hydrogels both in parallel and perpendicular directions. All hybrid hydrogels are viscoelastic, and a significantly increased percentage dissipation energy of polysaccharide-based hybrid hydrogels was observed compared to that of parent G-PEG hydrogel. In addition to percentage dissipation energy, stress relaxation property of all hybrid hydrogels was investigated under a constant 15% strain both in parallel and perpendicular directions in wet condition, and Table 4 and Fig. 4a, b demonstrate the stress relaxing properties in both directions. In line with percentage dissipation energy, all hybrid hydrogels showed stress relaxation behavior. Importantly, G-PEG-Ch depicted higher and faster (shorter stress relaxation half time, $\tau_{1/2}$, the time required by stress to

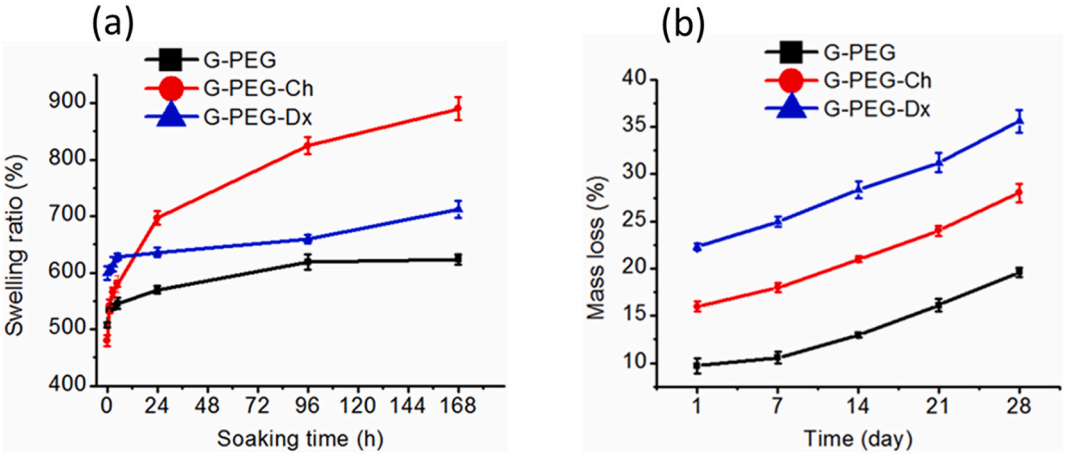

Fig. 2. (a) Swelling ratio (%) of the hybrid hydrogels carried out in distilled water at 37 °C as a function of soaking time and (b) mass loss (%) of the hybrid hydrogels during hydrolytic degradation at 37 °C for up to one month.

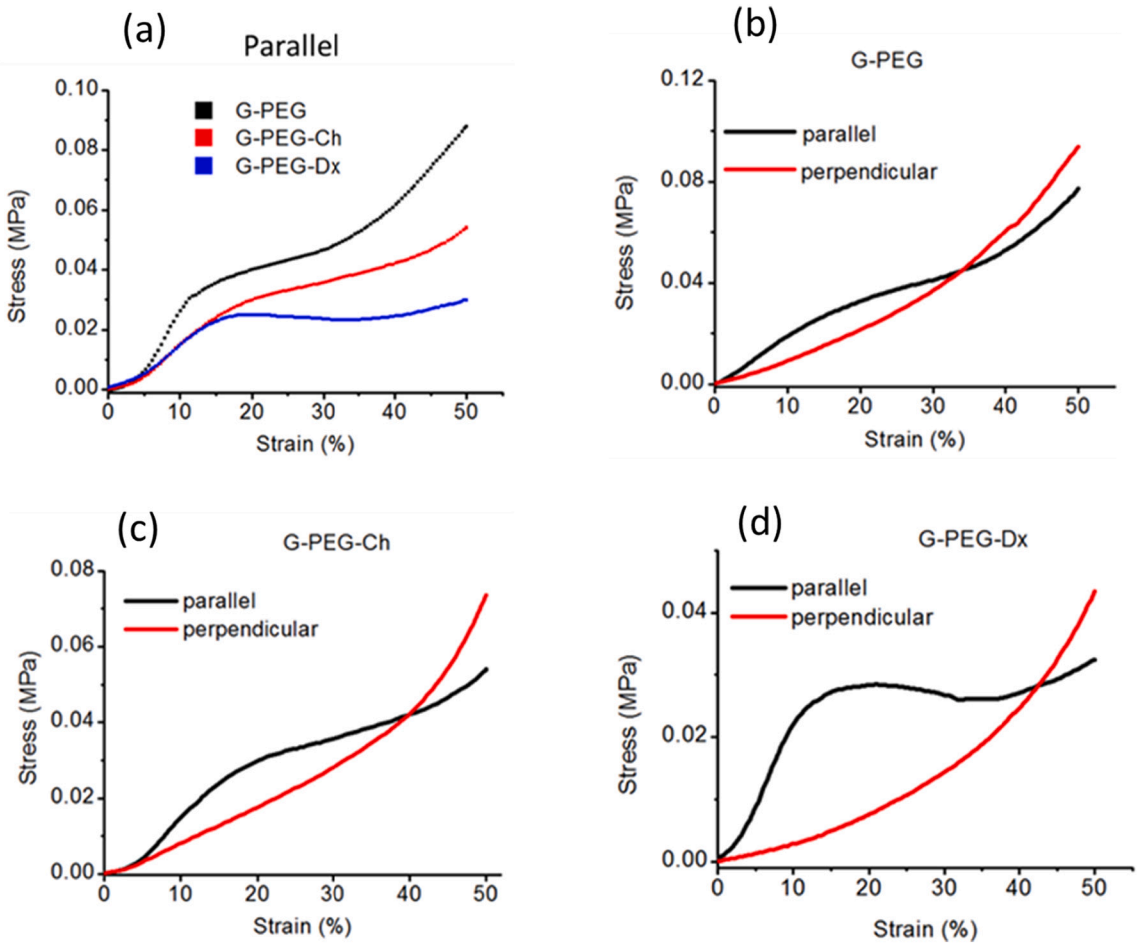

Fig. 3. Compressive mechanical properties of the hybrid hydrogels in the wet condition. (a) Compressive stress-strain curves showing comparison for all hybrid hydrogels in the parallel direction. Compressive stress-strain curves showing anisotropic properties for G-PEG (b), G-PEG-Ch (c) and G-PEG-Dx (d) hybrid hydrogels both in parallel and perpendicular directions.

Table 3
Compressive mechanical properties and dissipation energies of the anisotropic hybrid hydrogels both in parallel and perpendicular to the macroporous channels in wet condition.

Properties	G-PEG		G-PEG-Ch		G-PEG-Dx	
	Parallel	Perpendicular	Parallel	Perpendicular	Parallel	Perpendicular
Compressive elastic modulus (MPa)	0.33 ± 0.04	0.12 ± 0.03	0.25 ± 0.09	0.08 ± 0.03	0.28 ± 0.02	0.028 ± 0.006
Compressive stress at 50% strain (MPa)	0.08 ± 0.01	0.09 ± 0.01	0.07 ± 0.01	0.06 ± 0.01	0.06 ± 0.01	0.04 ± 0.01
Compression energy (kJ/m^3)	13.7 ± 4.2	14.5 ± 0.5	11.0 ± 1.5	8.8 ± 1.2	17.9 ± 4.3	5.4 ± 1.8
Relaxation energy (kJ/m^3)	8.7 ± 3.6	9.9 ± 1.2	6.02 ± 1.3	5.5 ± 0.6	7.4 ± 1.5	3.6 ± 0.8
Dissipation energy (kJ/m^3)	5.0 ± 0.6	4.6 ± 1.2	5.0 ± 0.9	3.3 ± 0.7	10.5 ± 3	1.8 ± 1.0
Dissipation energy (%)	38 ± 4	32 ± 5	46 ± 7	38 ± 3	58 ± 4	32 ± 8
Anisotropic ratio, $E_{\parallel}/E_{\perp}$	2.8		3.1		10.0	

Table 4
The stress relaxation properties of the anisotropic hybrid hydrogels held at 15% strain both in parallel and perpendicular to the macroporous channels in wet condition.

Hydrogels systems	Parallel compression (∥)		Perpendicular compression (⊥)	
	Relaxation [%]	$\tau_{1/2}$ [s]	Relaxation [%]	$\tau_{1/2}$ [s]
G-PEG	34 ± 4	1 ± 0.15	27 ± 2	1.9 ± 0.3
G-PEG-Ch	45 ± 5	0.8 ± 0.01	31 ± 2	1.6 ± 0.5
G-PEG-Dx	37 ± 4	1.5 ± 0.2	25 ± 4	2.5 ± 0.2

gradually decrease half of its initial stress (maximum) value) stress relaxation behavior compared to those of G-PEG and G-PEG-Dx hydrogels, and this higher stress relaxing response can be attributed to the molecular structure of chitosan. Notably, for all hybrid hydrogels, a higher and faster stress relaxation was observed in case of parallel compression, as compared to its counterpart (perpendicular) compression. This improved stress relaxing property in parallel compression might be due to the faster water movement within the hydrogel system.

3.3. Human BM-MSCs metabolic activity is modulated by scaffold composition

We evaluated hBM-MSCs metabolic activity after seeding on G-PEG,

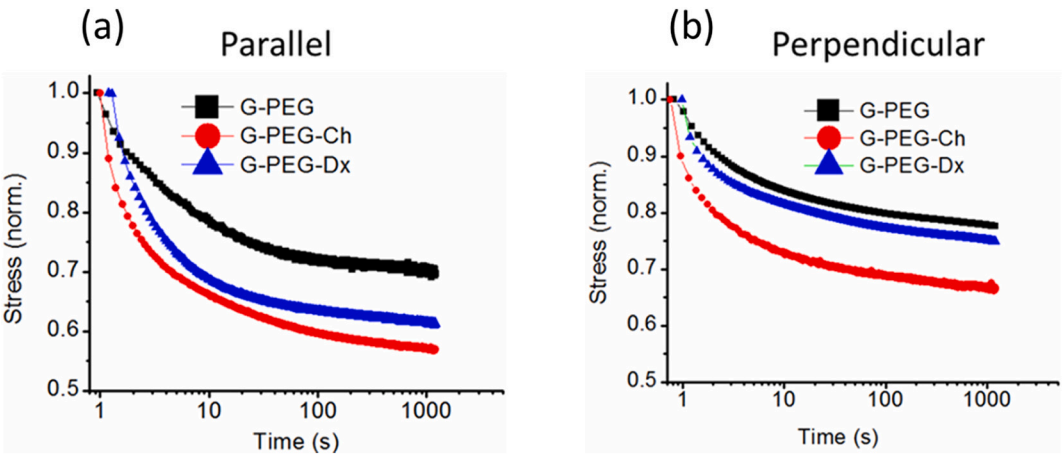

Fig. 4. Stress relaxation properties of the all anisotropic hybrid hydrogels held at 15% strain both in parallel (a) and perpendicular (b) directions in wet condition.

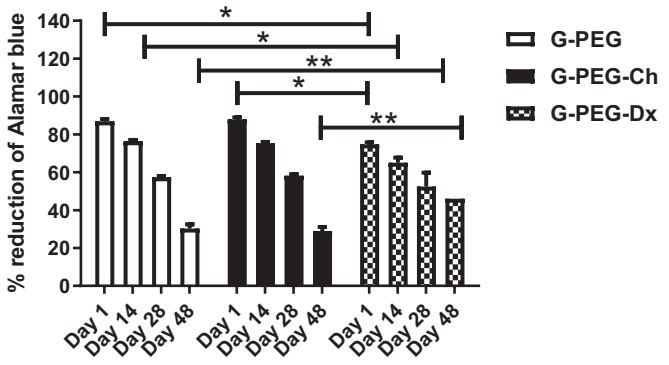

Fig. 5. Metabolic activity of hBM-MSCs chondrogenic differentiated on G-PEG, G-PEG-Ch and G-PEG-Dx. Metabolic activity was analysed at day 1, 14, 28 and 48 and data were expressed as mean ± SD of the % Alamar blue. Significant results between scaffolds were indicated as *p<0.05, **p<0.01.

GPEG-Ch and G-PEG-Dx at day 1, 14, 28 and 48. As shown in Fig. 5, already at day 1 until day 48 hBM-MSCs metabolic activity was already significantly lower when cells were seeded on G-PEG-Dx compare to G-PEG ($p < 0.05$and $p < 0.01$, respectively) or G-PEG-Ch ($p < 0.05$ and $p < 0.01$, respectively). Interestingly, we observed the same significant cell metabolic decrease activity also at day 14 ($p < 0.05$) when hBM-MSCs were grown on G-PEG compared to G-PEG-Dx scaffolds. By contrast, we did not observe any difference in cell metabolic activity when cells were grown on G-PEG or G-PEG-Ch.

3.4. Chondrogenic genes are differently modulated by scaffold composition

Then, we evaluated *COL1A1*, *COL2A1*, *COL9A1*, *COL11A1*, *SOX9*, *ACAN*, *COMP*, *MMP-13* and *COL10A1* genes expression of chondrogenic induced BM-MSCs on G-PEG, GPEG-Ch and G-PEG-Dx scaffolds. As shown in Fig. 6 the expression of the transcription factor *SOX9* and the ratio *COL2A1/COL1A1* was significantly higher in G-PEG-Ch scaffold ($p = 0.04$ and $p = 0.02$, respectively) compared to G-PEG-Dx, while the expression of *COL9A1* and *COMP* were significantly higher in G-PEG-Ch ($p = 0.03$ and $p = 0.03$, respectively) compared to G-PEG. Interestingly, the expression of *COL1A1* was significantly lower in G-PEG-Ch ($p = 0.04$) compared to G-PEG. The expression of *COL2A1*, *ACAN* and *COL11A1* did not show any difference among the scaffolds. The expression of hypertrophic marker *MMP-13* was significantly higher in G-PEG-Dx ($p = 0.02$ and $p = 0.002$, respectively) respect to both G-PEG-Ch and G-PEG, while COL10A1 was significantly higher in G-PEG-Dx ($p = 0.008$) compared to only G-PEG-Ch.

3.5. Cartilage proteoglycan expression and organization are modulated by scaffold composition

We firstly evaluated the infiltration of the cells into the scaffolds on haematoxylin-eosin stained sections. As shown in supplementary Fig. 1, at day 28 we evidenced that cells well infiltrated both on the border and inner parts of all the three scaffolds. Toluidine blue metachromatic staining was then used for the assessment of chondrogenic differentiated cells on the G-PEG, G-PEG-Ch and G-PEG-Dx scaffolds. As shown in Fig. 7A, the positive metachromatic staining of toluidine blue [35] (that stain in blue the nuclei and in pink-purple the proteoglycan) was clearly evident only in G-PEG (Fig. 7Aa, b) and G-PEG-Ch (Fig. 7Ac, d), but not in G-PEG-Dx (Fig. 7Ae, f) scaffold. In particular, both in G-PEG and G-PEG-Ch scaffolds mostly of the cells showed a round morphology and were embedded into the proteoglycan matrix (Fig. 7Ab, d), while in G-PEG-Dx we found a spindle-like cell morphology with a not evident extracellular matrix (Fig. 7Af). In G-PEG and G-PEG-Ch scaffolds the extracellular matrix was well organized with the presence of areas more or less mature (from pink to purple). Interestingly, we also noted the presence of cells completely embedded into the proteoglycan matrix that resemble the characteristics of the condron structure typical of mature cartilage. Von Kossa staining (supplementary Fig. 2) confirmed the absence of mineralized area into all three scaffolds.

Electron microscopy analysis also confirmed the presence of collagenic fibrils in the extracellular matrix (Fig. 7B) and a quantitative analysis evidenced a relative frequency percentage of collagenic fibrils with a diameter ranging from 10 to 49 nm (Fig. 7C).

4. Discussion

Designing and developing of novel scaffolding substrate remain a central piece of interest in the field of scaffold-based cartilage tissue engineering [1,4]. Due to their remarkable properties and cell-friendly perspective, hydrogels have emerged as the most promising candidate for tissue engineering application. Towards optimal performance, hydrogel development has been witnessing the emergence of a powerful set of new exciting design parameters to improve their ultimate utility. As such, we developed a novel 'softly-cum-simply' synthesis approach to fabricate hydrogels that were targeted to assist tissue regeneration. We exploited the synergy contribution between natural (gelatin, and polysaccharides chitosan and dextran) and synthetic polymer (polyethylene glycol) while keeping the threshold quantity of latter to avoid biocompatibility issue. Three hydrogels, namely, G-PEG, G-PEG-Ch and G-PEG-Dx were prepared via a green, simple, scalable and cost-effective

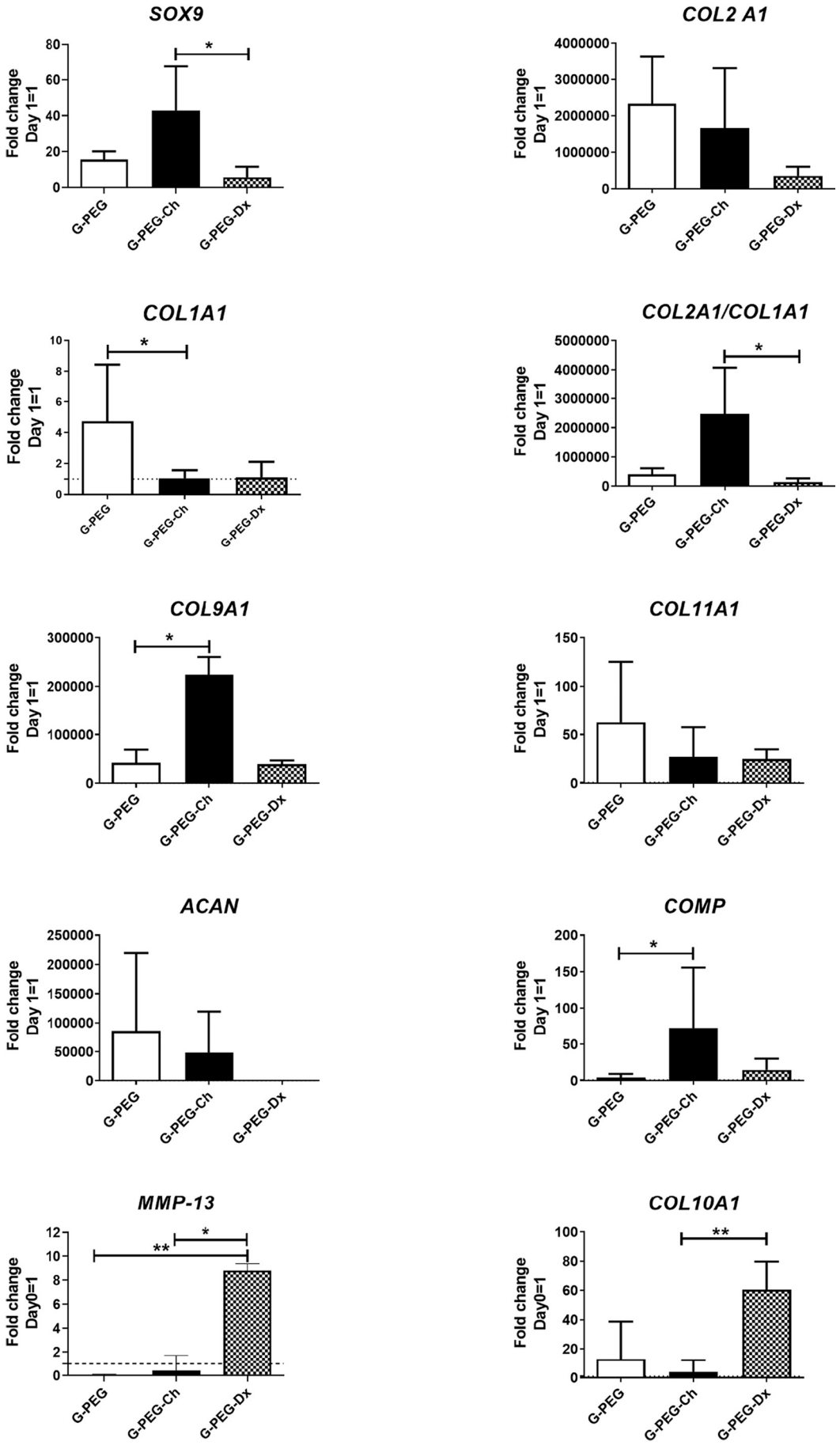

(caption on next page)

Fig. 6. Chondrogenic, fibrotic and hypertrophic markers on chondrogenic differentiated hBM-MSCs on G-PEG, G-PEG-Ch and G-PEG-Dx. *SOX9*, *COL2A1*, *COL1A1*, *COL2A1/COL1A1* ratio, *COL9A1*, *COL11A1*, *ACAN*, *COMP*, *MMP-13* and *COL10A1* genes were analysed at day 28 on hBM-MSCs chondrogenic differentiated on G-PEG, G-PEG-Ch and G-PEG-Dx scaffolds. Data were expressed as fold change Day 1 = 1. Significant results between scaffolds were indicated as *p < 0.05 or **p < 0.01.

synthesis procedure which mainly consists several sequential steps of grafting and cross-linking reactions, gelation, unidirectional freezing, freeze-drying and post curing process (Fig. 1a). The developed synthesis approach was versatile enough to accommodate a range of different polymers without perturbing the benign process conditions. The morphology of highly interconnected irregular spherical pores with macro and microporosities perpendicular to the freezing direction and macroporous channels along the freezing direction suggested that the prepared hybrid hydrogels have anisotropic architectures. The high porosity and interconnected pores with pore sizes ranging from 50 to 470 mm, is believed to ensure cell life and growth and to promote mass transportation including, nutrients supply and wastes disposal, vascularization and tissue regeneration [30,36].

Mechanical property of the scaffold is a key regulator to influence many cellular behaviors [37]. The collective mechanical behavior of all hydrogels was resemblance to the mechanics of anisotropic soft tissues. The incorporation of Ch and Dx into the G-PEG network results in a reduced availability of reactive primary amino groups of gelatin polymer chains to react with the epoxy groups of PEG. The resulting lower cross-linking density and higher hydrophilicity of the polysaccharide lead to slightly reduced stiffness of the G-PEG-Ch and G-PEG-Dx compared to that of parent G-PEG hydrogels. Furthermore, the incorporation of polysaccharides increased the anisotropic character of the hydrogels mainly for G-PEG-Dx.

Dissipation energy and stress relaxation are two main features that indicate viscoelastic response of the material, a time-dependent mechanical phenomenon which is reported to significantly influence many cellular behaviors, including cell spreading, proliferation and differentiation [37]. All hybrid hydrogels exhibited dissipation energy and stress relaxation behavior thus demonstrating their viscoelastic behavior. Importantly, polysaccharide incorporation significantly improved percentage dissipation energy of the hybrid hydrogels, suggesting improved viscoelastic behavior of G-PEG-Ch and G-PEG-Dx compared to that of parent hydrogel G-PEG. Furthermore, G-PEG-Ch exhibited higher and faster stress relaxation behavior than the other hydrogels, which could be a factor positively affecting rapid cell remodeling towards tissue regeneration.

Cell infiltration, metabolic activity, chondrogenic gene markers, proteoglycan, mineralization, cell morphology and collagenic fibrils were then evaluated to assess the chondrogenic potentiality of hBMSCs on these hybrid-hydrogels. We evidenced that hBMSCs only when chondrogenic differentiated on G-PEG, and G-PEG-Ch showed a significant higher decrease of metabolic activity that, as reported by different authors [24,38], represent the pre-requisite to cell differentiation. Moreover, as we previously reported [24], hBM-MSCs chondrogenic differentiation was also associated to a decrease of cellular proliferation. The presence of Dx on the scaffold seem to differently affect the metabolic activity of chondrogenic differentiated hBMSCs suggesting a peculiar role of this molecule. Dextran has hydroxyl groups that can be functionalized with reactive groups like thiol (SH) so permitting the formation of crosslinked hydrogels. It has been shown that Dx-SH crosslinked to PEG [39] was suitable for cartilage tissue engineering using articular bovine chondrocytes but not with embryonic stem cells-derived mesenchymal-like cells that did not adhere to this scaffold confirming the different role of Dx molecule. Interestingly, it has been also demonstrated that Dx sulfate inhibit mesenchymal precursor cells chondrogenic differentiation by reducing proteoglycan synthesis [40].

The analysis of typical chondrogenic genes evidenced a peculiar expression at day 28 on the different scaffolds. ACAN, *COL2A1* and *COL1A1* genes were higher in G-PEG and lower in G-PEG-Dx. By contrast, the transcriptor factor *SOX9* and *COL2A1/COL1A1* ratio were higher on G-PEG-Ch and lower in G-PEG-Dx indicating that the presence of Dx in the backbone of the scaffold could have negatively modulated the expression of the chondrogenic genes. Interestingly, G-PEG-Ch scaffold had a positive effect also on the minor proteins of the extracellular matrix like *COL9A1* and *COMP*. In line with our previous paper [24], proteoglycan staining with toluidine blue evidenced that chondrogenic differentiation well occurred on G-PEG and G-PEG-Ch but not on G-PEG-Dx scaffold, confirming that the composition of the scaffold is able to counteract important chondrogenic signalling, like TGFβ3, that we used in culture for hBM-MSCs chondrogenic induction. The presence of Dx in the scaffold seem to reduce its biological activity, hBM-MSC well penetrated through the scaffolds (supplementary Fig. 1) but showed a fibroblastic shape and were unable to produce organized extracellular matrix as occurred in absence or presence of Ch. It has been shown that Dx-sulphate shows a dose-dependent inhibition MSCs chondrogenesis [40]. Moreover, also using Dx-tyramine hydrogels it has been shown that have poor pro-chondrocytic activity [41] that seem improved only by treatment of the scaffolds with heparin or hyaluronic acid or mixing MSC with chondrocytes [42–45].Our data were also corroborated by a study that demonstrated on bovine chondrocytes embedded in Dx tyramine conjugated hydrogel an increase of collagen type 1 and reduction of collagen type 2 [42] confirming a negative effect on chondrogenic markers. However, a recent study using bioorthogonal chemistry for preparation of an injectable dextran based-hydrogel have demonstrated an enhanced chondrogenesis of rabbit adipose derived stem cells, suggesting that other chemical crosslinking reactions could affect cell differentiation and are not suitable for biomedical applications [23]. By contrast, the positive effects of different Ch-based scaffolds on chondrogenic differentiation of mesenchymal stem cells have been well documented in several studies [24,46,47]. Chitosan showing a structure like glycosaminoglycan (GAG) of the cartilage, when supplemented to different scaffold types seem to provide an environment that positively induce mesenchymal cells chondrogenic differentiation and increase the formation of the cartilaginous extracellular matrix.

Different papers [24,45,48] have focused on the regulation of hypertrophy and/or matrix calcification during MSCs chondrogenesis in hydrogels. We previously demonstrated [24] that condrogenic differentiated hMSCs in G-PEG-Ch reduced both the expression of hypertrophic and fibrotic markers (at gene and protein level) by increasing chondrogenesis. We confirmed that G-PEG-Ch was more efficient than G-PEG and G-PEG-Dx scaffolds in reducing the expression of the *COL10A1* and *MMP-13* hypertrophic markers and did not affect mineralization. It has been demonstrated [48] that hyaluronic acid hydrogel sulfation (at high concentration) promoted chondrogenesis by suppressing hypertrophy of encapsulated hMSC indicating, in line with our data, that a simple modification of a group on a common backbone could affect the properties of the scaffold and consequently its effect on cell chondrogenesis. Furthermore, it has been shown that the physicomechanical properties of the hydrogel mediated by alterations in the crosslinking density (i.e. mechanical stiffness and macromolecular diffusivity) must be considered in the context of the chondrogenic and hypertrophic differentiation. In particular, the increase in crosslinking density resulted in an overall decrease in cartilage matrix content and favoured hypertrophic differentiation and matrix calcification [45].

In light of this result the higher water uptake and lower mechanical stiffness of G-PEG-Ch, both indicating a lower cross-linking density than other hydrogels, are likely responsible for chondrogenic induction by reducing hypertrophic differentiation. It should also be highlighted that G-PEG-Ch exhibits higher and faster stress-relaxation properties than

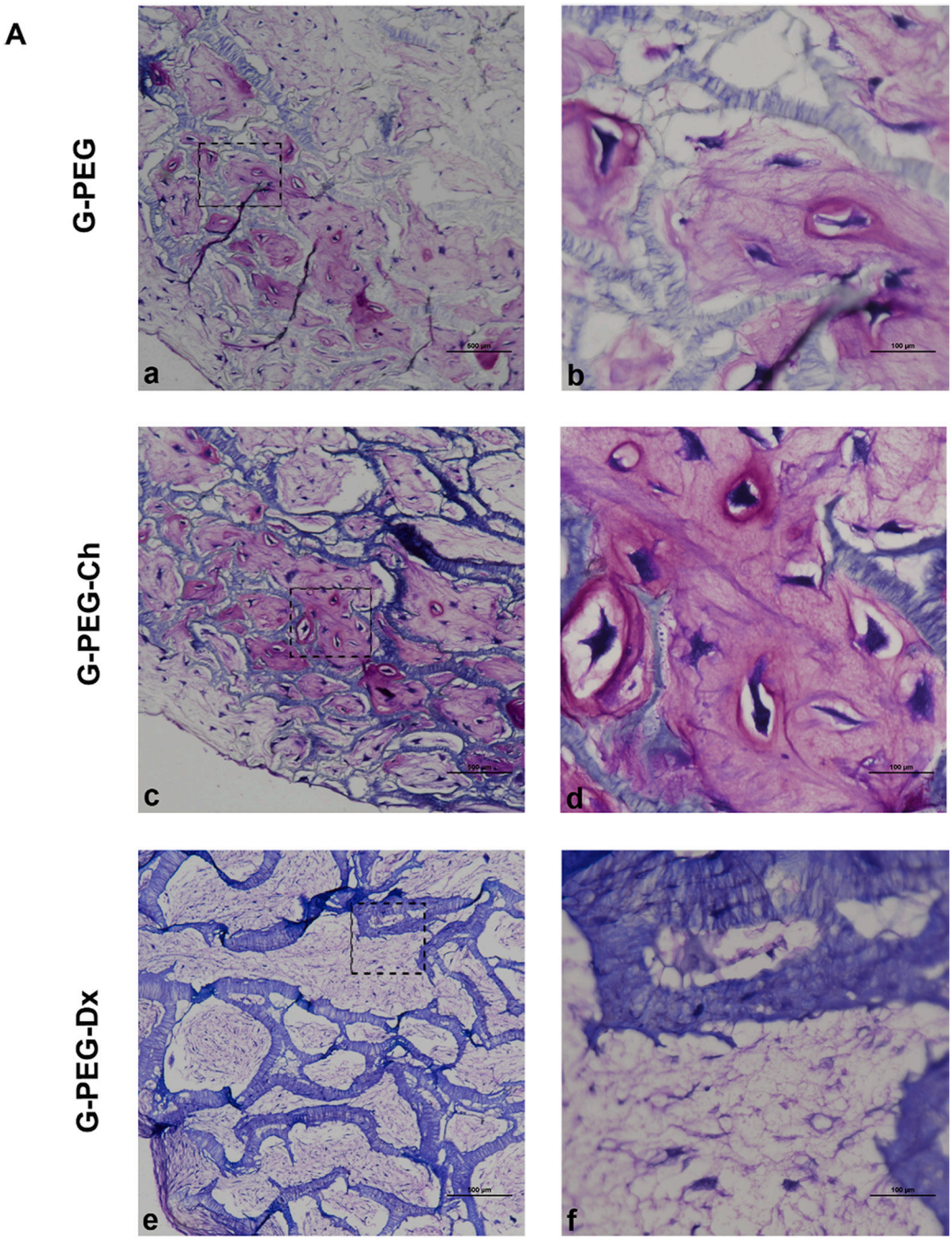

Fig. 7. Chondrogenic differentiation of hBM-MSCs on G-PEG, G-PEG-Ch and G-PEG-Dx. A. Toluidin blue staining of chondrogenic differentiated BM-MSCs on G-PEG (a, b), G-PEG-Ch (c, d) and G-PEG-Dx (e, f). Bar (a, c, e) = 500 μm, Bar (b, d, f) = 100 μm. B. Transmission electron microscopy of chondrogenic differentiated hBM-MSCs on G-PEG-Ch scaffold. Bar = 0.1 μm. C = cell, ECM = extracellular matrix, C. Quantification of collagenic fibrils of chondrogenic differentiated hBM-MSCs on G-PEG-Ch scaffold. Data are expressed as relative frequency percentage of collagenic fibrils with diameter ranging from 10 to 49 nm.

other scaffolds.

Interestingly, ultrastructural analysis of collagen fibrils in G-PEG-Ch scaffold evidenced that were randomly organized around the cells and showed a range of fibrils ranging from 10 to 49 nm. It has been shown [32] that healthy articular cartilage show collagen fibrils randomly aligned around the cells with a diameter from 10 to 130 nm that significantly increased in osteoarthritic cartilage, so confirming that G-PEG-Ch scaffold also contribute to the formation of collagenic fibrils similar to ones of healthy cartilage. Preliminary definition of the mechanical behavior and physical-chemical characteristics of the hybrid-hydrogels represent a strength of this study since could help to define in advance the potential of the scaffold for a specific cell differentiation process.

4.1. Conclusions

In conclusion, we evidenced the main differences among the hybrid hydrogels mechanical behavior, demonstrating that incorporation of Ch or Dx into the common G-PEG backbone resulted in slightly reduced stiffness compared to that of parent G-PEG hydrogel. Moreover, we found that G-PEG-Dx showed a significant increase of the anisotropic characteristics while G-PEG-Ch exhibited reduced crosslinking density, higher and faster stress relaxation behavior than the other hydrogels. These physical characteristics contribute to explain the different chondrogenic potential of hBM-MSCs. Indeed, hBM-MSCs on G-PEG-Dx were unable to differentiate while good chondrogenic differentiation was demonstrated on G-PEG and G-PEG-Ch. Moreover, G-PEG-Ch showed an increase of minor collagen proteins and the formation of collagen fibrils with dimension closed to healthy articular cartilage.

These data evidence that both mechanical stiffness and stress relaxation characteristics of the hydrogels are fundamental to guide chondrogenic differentiation of hBM-MSC into the scaffolds not inducing hypertrophy and mineralization, suggesting that these hybrid hydrogel features modulated hBM-MSCs differentiation process. Therefore, these scaffolds may be considered no more as a simple support, rather than active players in the differentiative and regenerative process.

Declaration of competing interest

The authors declare that they have no known competing financial interests or personal relationships that could have appeared to influence the work reported in this paper.

Acknowledgment

The authors are highly grateful to Gammaton (Como, Italy) for gamma sterilization of hydrogels.

Funding

Istituto Ortopedico Rizzoli fund “5 per mille 2018”.

Appendix A. Supplementary data

Supplementary data to this article can be found online at https://doi.org/10.1016/j.msec.2021.112175.

References

[1] E.V. Medvedeva, E.A. Grebenik, S.N. Gornostaeva, V.I. Telpuhov, A.V. Lychagin, P. S. Timashev, A.S. Chagin, Repair of damaged articular cartilage: current approaches and future directions, Int. J. Mol. Sci. 19 (8) (2018).
[2] E.A. Makris, A.H. Gomoll, K.N. Malizos, J.C. Hu, K.A. Athanasiou, Repair and tissue engineering techniques for articular cartilage, Nat. Rev. Rheumatol. 11 (1) (2015) 21–34.
[3] J.D. Lamplot, K.A. Schafer, M.J. Matava, Treatment of failed articular cartilage reconstructive procedures of the knee: a systematic review, Orthop. J. Sports Med. 6 (3) (2018), 2325967118761871.
[4] G.I. Im, C.S. Cho, Updates in cartilage tissue regeneration, Tissue Eng. Regen. Med. 16 (4) (2019) 325–326.
[5] Y.M. Lin, J. Lee, J.F.Y. Lim, M. Choolani, J.K.Y. Chan, S. Reuveny, S.K.W. Oh, Critical attributes of human early mesenchymal stromal cell-laden microcarrier constructs for improved chondrogenic differentiation, Stem Cell Res Ther 8 (1) (2017) 93.
[6] D. Eyre, Collagen of articular cartilage, Arthritis Res. 4 (1) (2002) 30–35.
[7] N.P. Cohen, R.J. Foster, V.C. Mow, Composition and dynamics of articular cartilage: structure, function, and maintaining healthy state, J. Orthop. Sports Phys. Ther. 28 (4) (1998) 203–215.
[8] M. Mendler, S.G. Eich-Bender, L. Vaughan, K.H. Winterhalter, P. Bruckner, Cartilage contains mixed fibrils of collagen types II, IX, and XI, J. Cell Biol. 108 (1) (1989) 191–197.
[9] P. Parsons, S.J. Gilbert, A. Vaughan-Thomas, D.A. Sorrell, R. Notman, M. Bishop, A. J. Hayes, D.J. Mason, V.C. Duance, Type IX collagen interacts with fibronectin providing an important molecular bridge in articular cartilage, J. Biol. Chem. 286 (40) (2011) 34986–34997.
[10] A.J. Sophia Fox, A. Bedi, S.A. Rodeo, The basic science of articular cartilage: structure, composition, and function, Sports Health 1 (6) (2009) 461–468.
[11] F. Burla, J. Tauber, S. Dussi, J. van Der Gucht, G.H. Koenderink, Stress management in composite biopolymer networks, Nat. Phys. 15 (6) (2019) 549.
[12] B. Balakrishnan, R. Banerjee, Biopolymer-based hydrogels for cartilage tissue engineering, Chem. Rev. 111 (8) (2011) 4453–4474.
[13] Q. Chen, X. Shao, P. Ling, F. Liu, G. Han, F. Wang, Recent advances in polysaccharides for osteoarthritis therapy, Eur. J. Med. Chem. 139 (2017) 926–935.
[14] D.L. Nettles, S.H. Elder, J.A. Gilbert, Potential use of chitosan as a cell scaffold material for cartilage tissue engineering, Tissue Eng. 8 (6) (2002) 1009–1016.
[15] S. Mohebbi, M.N. Nezhad, P. Zarrintaj, S.H. Jafari, S.S. Gholizadeh, M.R. Saeb, M. Mozafari, Chitosan in biomedical engineering: a critical review, Curr. Stem Cell Res. Ther. 14 (2) (2019) 93–116.
[16] G. Sun, X. Zhang, Y.I. Shen, R. Sebastian, L.E. Dickinson, K. Fox-Talbot, M. Reinblatt, C. Steenbergen, J.W. Harmon, S. Gerecht, Dextran hydrogel scaffolds enhance angiogenic responses and promote complete skin regeneration during burn wound healing, Proc. Natl. Acad. Sci. U. S. A. 108 (52) (2011) 20976–20981.
[17] M.H. Lee, D. Boettiger, R.J. Composto, Biomimetic carbohydrate substrates of tunable properties using immobilized dextran hydrogels, Biomacromolecules 9 (9) (2008) 2315–2321.
[18] L.S. Ferreira, S. Gerecht, J. Fuller, H.F. Shieh, G. Vunjak-Novakovic, R. Langer, Bioactive hydrogel scaffolds for controllable vascular differentiation of human embryonic stem cells, Biomaterials 28 (17) (2007) 2706–2717.
[19] G. Sun, Y.I. Shen, S. Kusuma, K. Fox-Talbot, C.J. Steenbergen, S. Gerecht, Functional neovascularization of biodegradable dextran hydrogels with multiple angiogenic growth factors, Biomaterials 32 (1) (2011) 95–106.
[20] X. Wang, Z. Li, T. Shi, P. Zhao, K. An, C. Lin, H. Liu, Injectable dextran hydrogels fabricated by metal-free click chemistry for cartilage tissue engineering, Mater. Sci. Eng. C Mater. Biol. Appl. 73 (2017) 21–30.
[21] R. Jin, L.S. Moreira Teixeira, P.J. Dijkstra, Z. Zhong, C.A. van Blitterswijk, M. Karperien, J. Feijen, Enzymatically crosslinked dextran-tyramine hydrogels as injectable scaffolds for cartilage tissue engineering, Tissue Eng. Part A 16 (8) (2010) 2429–2440.
[22] T. Ito, Y. Yeo, C.B. Highley, E. Bellas, D.S. Kohane, Dextran-based in situ cross-linked injectable hydrogels to prevent peritoneal adhesions, Biomaterials 28 (23) (2007) 3418–3426.
[23] L. Fan, C. Lin, P. Zhao, X. Wen, G. Li, An injectable bioorthogonal dextran hydrogel for enhanced chondrogenesis of primary stem cells, Tissue Eng. Part C Methods 24 (9) (2018) 504–513.
[24] C. Manferdini, E. Gabusi, L. Sartore, K. Dey, S. Agnelli, C. Almici, A. Bianchetti, N. Zini, D. Russo, F. Re, E. Mariani, G. Lisignoli, Chitosan-based scaffold counteracts hypertrophic and fibrotic markers in chondrogenic differentiated mesenchymal stromal cells, J. Tissue Eng. Regen. Med. 13 (10) (2019) 1896–1911.
[25] S. Goren, Y. Koren, X. Xu, A. Lesman, Elastic anisotropy governs the range of cell-induced displacements, Biophys. J. 118 (5) (2020) 1152–1164.
[26] S.D. McCullen, H. Autefage, A. Callanan, E. Gentleman, M.M. Stevens, Anisotropic fibrous scaffolds for articular cartilage regeneration, Tissue Eng. Part A 18 (19–20) (2012) 2073–2083.
[27] A. Arora, A. Kothari, D.S. Katti, Pore orientation mediated control of mechanical behavior of scaffolds and its application in cartilage-mimetic scaffold design, J. Mech. Behav. Biomed. Mater. 51 (2015) 169–183.
[28] R.F. MacBarb, A.L. Chen, J.C. Hu, K.A. Athanasiou, Engineering functional anisotropy in fibrocartilage neotissues, Biomaterials 34 (38) (2013) 9980–9989.
[29] W.J. Li, R.L. Mauck, J.A. Cooper, X. Yuan, R.S. Tuan, Engineering controllable anisotropy in electrospun biodegradable nanofibrous scaffolds for musculoskeletal tissue engineering, J. Biomech. 40 (8) (2007) 1686–1693.
[30] K. Dey, S. Agnelli, F. Re, D. Russo, G. Lisignoli, C. Manferdini, S. Bernardi, E. Gabusi, L. Sartore, Rational design and development of anisotropic and mechanically strong gelatin-based stress relaxing hydrogels for Osteogenic/Chondrogenic differentiation, Macromol. Biosci. 19 (8) (2019), e1900099.
[31] C.R. Kothapalli, M.T. Shaw, M. Wei, Biodegradable HA-PLA 3-D porous scaffolds: effect of nano-sized filler content on scaffold properties, Acta Biomater. 1 (6) (2005) 653–662.
[32] N. Tanaka, T. Tashiro, Y. Katsuragawa, M. Sawabe, H. Furukawa, N. Fukui, Expression of minor cartilage collagens and small leucine rich proteoglycans may be relatively reduced in osteoarthritic cartilage, BMC Musculoskelet. Disord. 20 (1) (2019) 232.

[33] K. Dey, S. Agnelli, L. Sartore, Effects of gamma sterilization on the physicomechanical and thermal properties of gelatin-based novel hydrogels, Polym. Eng. Sci. 59 (12) (2019) 2533–2540.
[34] K. Dey, S. Agnelli, M. Serzanti, P. Ginestra, G. Scari, P. Dell'Era, L. Sartore, Preparation and properties of high performance gelatin-based hydrogels with chitosan or hydroxyethyl cellulose for tissue engineering applications, Int. J. Polym. Mater. 68 (4) (2019) 183–192.
[35] N.L. Bergholt, H. Lysdahl, M. Lind, C.B. Foldager, A standardized method of applying toluidine blue metachromatic staining for assessment of chondrogenesis, Cartilage 10 (3) (2019) 370–374.
[36] S.H. Oh, I.K. Park, J.M. Kim, J.H. Lee, In vitro and in vivo characteristics of PCL scaffolds with pore size gradient fabricated by a centrifugation method, Biomaterials 28 (9) (2007) 1664–1671.
[37] K. Dey, S. Agnelli, L. Sartore, Dynamic freedom: substrate stress relaxation stimulates cell responses, Biomater. Sci. 7 (3) (2019) 836–842.
[38] G. Pattappa, H.K. Heywood, J.D. de Bruijn, D.A. Lee, The metabolism of human mesenchymal stem cells during proliferation and differentiation, J. Cell. Physiol. 226 (10) (2011) 2562–2570.
[39] J.M. Jukes, L.J. van der Aa, C. Hiemstra, T. van Veen, P.J. Dijkstra, Z. Zhong, J. Feijen, C.A. van Blitterswijk, J. de Boer, A newly developed chemically crosslinked dextran-poly(ethylene glycol) hydrogel for cartilage tissue engineering, Tissue Eng. Part A 16 (2) (2010) 565–573.
[40] P. Ghosh, J. Wu, S. Shimmon, A.C. Zannettino, S. Gronthos, S. Itescu, Pentosan polysulfate promotes proliferation and chondrogenic differentiation of adult human bone marrow-derived mesenchymal precursor cells, Arthritis Res. Ther. 12 (1) (2010) R28.
[41] L.S. Moreira Teixeira, J.C. Leijten, J.W. Wennink, A.G. Chatterjea, J. Feijen, C.A. van Blitterswijk, P.J. Dijkstra, M. Karperien, The effect of platelet lysate supplementation of a dextran-based hydrogel on cartilage formation, Biomaterials 33 (14) (2012) 3651–3661.
[42] R. Jin, L.S. Moreira Teixeira, P.J. Dijkstra, C.A. van Blitterswijk, M. Karperien, J. Feijen, Chondrogenesis in injectable enzymatically crosslinked heparin/dextran hydrogels, J. Control. Release 152 (1) (2011) 186–195.
[43] R. Jin, L.S.M. Teixeira, P.J. Dijkstra, C.A. van Blitterswijk, M. Karperien, J. Feijen, Enzymatically-crosslinked injectable hydrogels based on biomimetic dextran-hyaluronic acid conjugates for cartilage tissue engineering, Biomaterials 31 (11) (2010) 3103–3113.
[44] C. Acharya, A. Adesida, P. Zajac, M. Mumme, J. Riesle, I. Martin, A. Barbero, Enhanced chondrocyte proliferation and mesenchymal stromal cells chondrogenesis in coculture pellets mediate improved cartilage formation, J. Cell. Physiol. 227 (1) (2012) 88–97.
[45] L. Bian, C. Hou, E. Tous, R. Rai, R.L. Mauck, J.A. Burdick, The influence of hyaluronic acid hydrogel crosslinking density and macromolecular diffusivity on human MSC chondrogenesis and hypertrophy, Biomaterials 34 (2) (2013) 413–421.
[46] Y. Huang, D. Seitz, F. Konig, P.E. Muller, V. Jansson, R.M. Klar, Induction of articular chondrogenesis by chitosan/hyaluronic-acid-based biomimetic matrices using human adipose-derived stem cells, Int. J. Mol. Sci. 20 (18) (2019).
[47] L.P. Merlin Rajesh Lal, G.K. Suraishkumar, P.D. Nair, Chitosan-agarose scaffolds supports chondrogenesis of human Wharton's jelly mesenchymal stem cells, J. Biomed. Mater. Res. A 105 (7) (2017) 1845–1855.
[48] Q. Feng, S. Lin, K. Zhang, C. Dong, T. Wu, H. Huang, X. Yan, L. Zhang, G. Li, L. Bian, Sulfated hyaluronic acid hydrogels with retarded degradation and enhanced growth factor retention promote hMSC chondrogenesis and articular cartilage integrity with reduced hypertrophy, Acta Biomater. 53 (2017) 329–342.